

# Electrolyte-Controlled Redox Conductivity and n-Type Doping in Poly(bis-EDOT-pyridine)s<sup>†</sup>

C. J. DuBois,<sup>‡</sup> Khalil A. Abboud, and John R. Reynolds\*

Department of Chemistry and Center for Macromolecular Science and Engineering, University of Florida, Gainesville, Florida 32611

Received: October 7, 2003; In Final Form: January 19, 2004

We report the use of electrolyte variations as a means to actively control redox and n-type doping processes in  $\pi$ -conjugated electroactive polyheterocycles. Specifically, a series of donor–acceptor bis-EDOT-pyridine polymers, poly[2,5-bis-(2,3-dihydro-thieno[3,4-*b*][1,4]dioxin-5-yl)-pyridine] (PBEDOT-Pyr) and poly[5,8-bis(3-dihydro-thieno[3,4-*b*][1,4]dioxin-5-yl)-2,3-diphenyl-pyrido[3,4-*b*]pyrazine] (PBEDOT-PyrPyr(Ph)<sub>2</sub>), have been investigated. The use of soft, bulky cations, such as *n*-alkylammonium, allows true n-type doping to be observed in cyclic voltammetry, differential-pulse voltammetry, and in situ conductance experiments. Color changes are also observed upon conversion of the polymers from their neutral to reduced states. Hard, electrophilic cations, such as lithium and sodium, induce minimal current and conductivity responses for these polymeric systems. This “pinning” of the cation–anion pair causes a decrease in the electrochemical and conductivity response. Optical changes upon reduction are observed that are distinct from the *n*-alkylammonium salts, indicating the lack of charge carrier formation and illustrating that reductive processes are not indicative of true doping in simple electrochemical experiments.

## Introduction

Current work in the field of conjugated electroactive polymers has led to the use of these systems in diverse applications such as transistors,<sup>1</sup> sensing,<sup>2</sup> emission,<sup>3</sup> patterning,<sup>4</sup> charge storage,<sup>5</sup> and photovoltaic<sup>6</sup> and electrochromic devices.<sup>7</sup> To better understand the fundamental science behind the structure–property relationships of the polymers used in such applications, the nature of the charge carriers, whether positive (hole transport or p-doping) or negative (electron transport or n-doping), has become increasingly important. The bulk of these systems exhibit p-type doping. Because of the inherent instability of the n-type doped redox state to water and oxygen, these systems have seen little real world utility.<sup>8</sup> One method of increasing the stability of the n-type doped state is to incorporate donor–acceptor (D–A) units into the polymer backbone.

The use of the D–A approach is designed to allow a single polymer system to undergo either transport mechanism easily in an electrochemical window that precludes degradation effects of the polymer associated with water and oxygen. Facile derivatization of these D–A systems has resulted in some the most successful results to date to control the position of the polymer system's valence and conduction bands and with that control, the ability to modulate the system's electronic and optical properties.<sup>9</sup> D–A systems also have seen utility in a variety of applications including n-channel field effect transistors, light-emitting diodes, and photovoltaics.<sup>10</sup> Incorporation of these D–A effects into a polymeric system allows for low band gaps to be achieved and application stable p- and n-type doped states to be accessible. Control over the position of the

valence band (HOMO) by incorporation of an electron-rich EDOT unit, for example, allows for the valence band to be relatively high in energy and oxidation to occur readily. As discussed in this paper, the position of the conduction band (LUMO) can be lowered by introduction of an electron-accepting unit such that reduction occurs easily. Use of an electron-poor pyridine or pyrido[3,4-*b*]pyrazine positions the conduction band (LUMO) in energy space such that reduction occurs easily. Control over the position of the energy levels allows for the band gap to be raised or lowered to meet the needs of the desired application.

Our group has previously investigated the electrochemical and optical properties of poly[2,5-bis-(2,3-dihydro-thieno[3,4-*b*][1,4]dioxin-5-yl)-pyridine] (PBEDOT-Pyr, **1**) and poly[5,8-bis(3-dihydro-thieno[3,4-*b*][1,4]dioxin-5-yl)-2,3-diphenyl-pyrido[3,4-*b*]pyrazine] (PBEDOT-PyrPyr(Ph)<sub>2</sub>, **2**) using the tetra-*n*-butylammonium perchlorate (TBAP) electrolyte system as shown in Figure 1.<sup>11</sup> Poly(**2**) has been shown to efficiently switch between four discrete redox states and has the smallest p- to n-type doping conductance ratio reported to date.<sup>11b</sup>

In this work we present results on the use of four cations to control the redox properties of these two polymer systems: tetra-*n*-butylammonium (TBA<sup>+</sup>), tetra-*n*-ethylammonium (TEA<sup>+</sup>), sodium (Na<sup>+</sup>), and lithium (Li<sup>+</sup>). Variation of the cation in the electrolyte allows unique electrolyte effects to be demonstrated in the same polymer system.<sup>12</sup> For the first time we demonstrate that the use of TBAP and TEAP allows for both poly(**1**) and poly(**2**) to display “true” n-type doping, while more electrophilic hard metal cations such as lithium and sodium display redox conductivity behavior.<sup>13</sup> This cation-specific behavior is known for a variety of electrochemically doped systems that include polythiophene<sup>14</sup> and polyacetylene.<sup>15</sup> The inability of alkaline cations to serve as dopants is due to “pinning” of the doped state and lack of delocalization of the charge carrier along the polymeric backbone. Previous work has shown, in fact, that

<sup>†</sup> Part of the special issue “Alvin L. Kwiram Festschrift”.

\* Corresponding author. Phone: 352-392-9151. Fax: 352-392-9741. E-mail: reynolds@chem.ufl.edu.

<sup>‡</sup> Current address: E. I. DuPont de Nemours and Co., Inc., Central Research and Development, Experimental Station, Wilmington, DE 19880-0328.

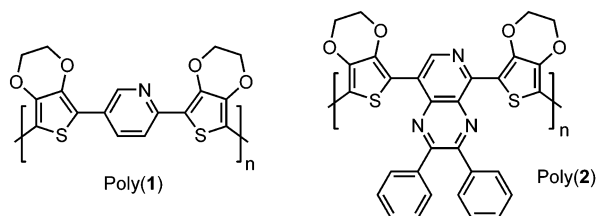


Figure 1. Repeat unit structure of D–A–D effective copolymers.

alkaline cations actually lead to hydrogenation of the double bonds in the  $\pi$ -conjugated systems.<sup>14</sup>

### Experimental Section

Monomers **1** and **2** were synthesized according to the published procedure.<sup>11b</sup> Tetra-*n*-butylammonium perchlorate and tetra-*n*-ethylammonium perchlorate were synthesized by the metathesis of concentrated perchloric acid and the appropriate *n*-alkylammonium bromide. Recrystallization three times from isopropyl alcohol followed by drying in a vacuum oven for 3 days gave the pure electrolyte salts. Sodium perchlorate and lithium perchlorate were melted under high vacuum to remove the waters of hydration. Each electrolyte was immediately transferred under vacuum to an argon-filled drybox.

**Electrochemistry.** Cyclic voltammetry (CV) and differential-pulse voltammetry (DPV) were performed using an EG&G Princeton Applied Research model 273A potentiostat/galvanostat. Polymer films were electrochemically synthesized using cyclic voltammetry on platinum disk electrodes (0.02 cm<sup>2</sup>) from 5 mM monomer/0.1 M tetra-*n*-butylammonium perchlorate solutions in a 1:1 mixture of acetonitrile and dichloromethane at 100 mV s<sup>-1</sup>. The resulting polymer film was then washed with copious amounts 0.1 M TBAP in acetonitrile to remove any residual monomer. The films were not allowed to dry out in order to prevent collapse. The polymer films were potential cycled a minimum of 20 times at 100 mV s<sup>-1</sup> over their redox active region (−0.1 to +1.25 V for p-doping and −1.0 to −2.3 V for n-doping of polymer **1**, for example) to allow for break-in.<sup>14</sup> CV and DPV examination of each electrolyte system used the same polymer film with this break-in cycling used to condition the film for each electrolyte system. The polymer films were relatively stable during this extensive cycling retaining at least 75% of their peak anodic and cathodic currents after 200 switches when examined in the initial TBAP electrolyte solution. Fresh polymer films were electrosynthesized using the same conditions as described above for the DPV experiments. The DPV experiments used a step size of 2 mV, a step time of 0.0167 s, and an amplitude of 100 mV. A coiled platinum wire was used as a counter electrode and silver wire as a reference. Before and after each experiment, the silver pseudoreference was calibrated versus the ferrocene redox couple and then adjusted to match the SCE reference potential. All electrochemical experiments were conducted in an argon-filled glovebox (H<sub>2</sub>O and O<sub>2</sub> concentrations less than 1 ppm).

**In Situ Conductance.** In situ conductance measurements were performed with the above potentiostat/galvanostat in tandem with a Pine bipotentiostat model AFCBP1 using a modification of the steady-state procedure described by Wrighton et al.<sup>16</sup> This procedure called for the working electrode of the bipotentiostat to serve as the gate and was “shorted” with the working electrode of the potentiostat/galvanostat and connected to one side of the IME bus. The other side of the IME bus was connected to the shorted reference and counter of the potentiostat/galvanostat and served as the drain. The reference and counter electrodes of the bipotentiostat served as the

corresponding working and counter electrodes of the electrochemical cell. The electrical resistance of the polymer was determined at 50 mV intervals by holding the gate at the desired potential for 1–2 min to allow for equilibrium conditions and sweeping the drain potential from +20 mV to −20 mV at a sweep rate of 1 mV s<sup>-1</sup>. The slope of the resulting line ( $E_{\text{drain}}$  vs  $I_{\text{drain}}$ ) was obtained by using linear regression techniques ( $R^2$  values greater than 0.99 for each case) and was taken to be the conductance of the film.

Platinum-based interdigitated microelectrodes were supplied by Dr. Giovanni C. Fiaccabrino, Institute of Microtechnology (IMT), University of Neuchâtel. The IMEs consisted of a printed circuit board encapsulated in epoxy with the electrode area having 5  $\mu\text{m}$  line widths, 5  $\mu\text{m}$  gaps, 1 mm lengths, and 50 pairs of bands. A layer of silicon nitride on top of the platinum bands served as a passivation layer to limit polymer growth to the interdigitation region only. In situ conductivity experiments were performed on the freshly polymerized polymer after each system had been broken in as described above in the electrochemistry section. All polymer films were determined to be more resistive than the leads ( $R = 150 \Omega$ ).

Before and after each experiment, the silver pseudoreference was calibrated versus the ferrocene redox couple and then adjusted to match the SCE reference potential.<sup>17</sup> All electrochemical experiments were conducted in an argon-filled glovebox (H<sub>2</sub>O and O<sub>2</sub> concentrations less than 1 ppm). A coiled platinum wire was used as a counter electrode and silver wire as the reference. The polymer films were synthesized by potentiostatic growth of the appropriate monomer solution until 4 mC of charge had passed at +1.2 V.

**X-ray Crystallography.** Single crystals of monomer **2** were grown from a filtered, saturated solution of the monomer in benzene-*d*<sub>6</sub>. Data were collected at 173 K on a Siemens SMART PLATFORM equipped with a CCD area detector and a graphite monochromator utilizing Mo K $\alpha$  radiation ( $\lambda = 0.71073 \text{ \AA}$ ). Cell parameters were refined using up to 8192 reflections. A full sphere of data (1850 frames) was collected using the  $\omega$ -scan method (0.3° frame width). The first 50 frames were remeasured at the end of data collection to monitor instrument and crystal stability (maximum correction on  $I$  was <1%). Absorption corrections by integration were applied based on measured indexed crystal faces.

The structure was solved by the Direct Methods in SHELX-TL6,<sup>18</sup> and refined using full-matrix least squares. The non-H atoms were treated anisotropically, whereas the hydrogen atoms were calculated in ideal positions and were riding on their respective carbon atoms. The space group,  $P2_12_12_1$ , is chiral, thus only one enantiomer exists in the crystal. The correct enantiomer is reported here judging by the value of a Flack parameter of −0.02(11). A total of 361 parameters were refined in the final cycle of refinement using 13405 reflections with  $I > 2\sigma(I)$  to yield  $R_1$  and  $wR_2$  of 5.32% and 11.92%, respectively. Refinement was done using  $F^2$ .

### Results and Discussion

**Polymer Cyclic Voltammetry.** As can be seen in Figure 2, the reproducible cyclic voltammetry (CV) behavior upon oxidation for each polymer is very similar for each electrolyte system used. This behavior is expected as the only difference between the four electrolytes is the cation. Onsets and associated  $E_{1/2}$  values are consistent with the behavior of other p-type doping polymers including PEDOT.<sup>19</sup> The relative onsets and  $E_{1/2}$  values are expected to differ slightly for each electrolyte system because of the hard–soft behavior of each electrolyte

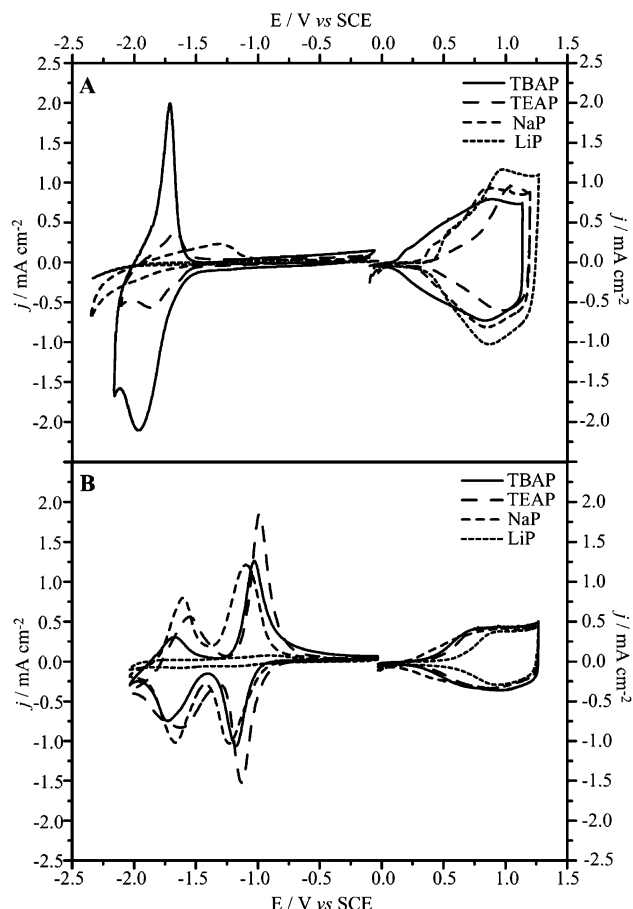


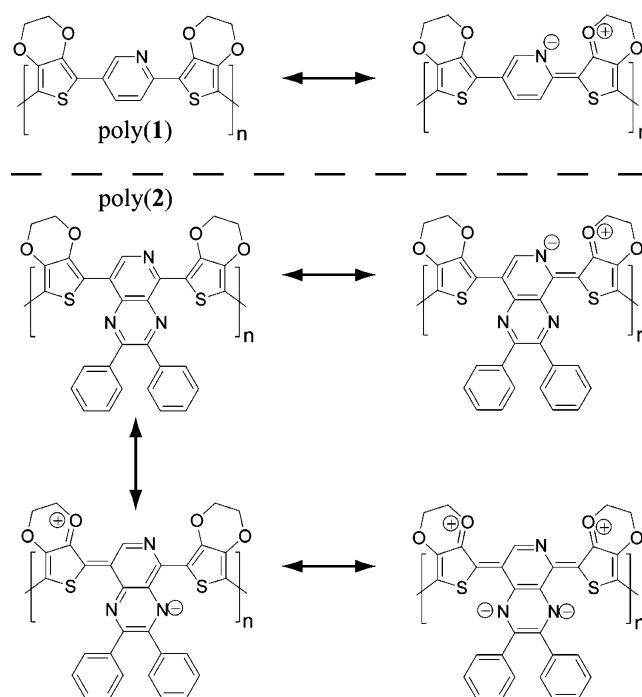
**Figure 2.** Cyclic voltammetry of poly(1) (A) and poly(2) (B) in 0.1 M monomer-free electrolyte solution. The solid line is TBAP, the large dashed line is TEAP, the medium dashed line is NaP, and the small dashed line is LiP. Each polymer was grown cyclically on Pt, rinsed with the appropriate electrolyte solution, and scanned 20 times over the entire potential range to “break-in” the film. (Data shown for TBAP are reprinted with permission from ref 11b. Copyright 2002 Wiley-VCH.)

cation–anion pair. As shown in Figure 2A, poly(1) has an  $E_{1/2}$  value of +1.1 V for the TEAP electrolyte system and +0.9 V for the TBAP electrolyte system. The same relative current density as NaP is displayed. NaP has an  $E_{1/2}$  at +0.9 V. LiP, the hardest cation–anion pair, exhibits the largest current densities with an onset for oxidation at +0.4 V and an  $E_{1/2}$  centered at +0.9 V. Color changes upon conversion of the neutral polymer (red) to the oxidized form (navy blue) occur for all the electrolytes used. Since the color change implies a doping process, each electrolyte system behaves as expected since perchlorate is the predominant anion that charge compensates in the doped film.

Of the four electrolyte systems upon reduction, though, only TBAP and TEAP exhibit current responses at negative potentials. Upon reduction, poly(1) is converted from the red neutral form to the sky blue n-type doped form. With the both the TBAP and TEAP systems an  $E_{1/2}$  value of –1.6 V is seen. The expected color changes with this electrolyte are also observed. NaP does display a visible current density, but the  $E_{1/2}$  values could not be calculated because of the ever-increasing current density. The current density associated with LiP is indiscernible from background current. Neither NaP nor LiP display color changes upon reduction hinting that there is no mobility of the charge carriers and thus no color change due to pinning.<sup>20</sup>

As seen in Figure 2B for poly(2), current densities associated with oxidation are of the same relative magnitude for all of the

### SCHEME 1: Donor–Acceptor Behavior of the Neutral Electrochemically Polymerized Polymers



electrolyte systems including TBAP. The increase in acceptor strength only slightly affects the onset of oxidation (valence band level). NaP has the earliest oxidation onset at +0.2 V and displays an  $E_{1/2}$  of +1.0 V. TBAP follows with its onset at +0.4 V. TEAPs oxidation onset is slightly more positive at +0.5 V and an  $E_{1/2}$  of +1.0 V. LiP, the hardest cation–ion pair, has the most positive onset of +0.7 V and the  $E_{1/2}$  was indiscernible because of an ever-increasing current as the potential was swept more positive.

As with poly(1), poly(2) displays visible current densities with TBA<sup>+</sup> and TEA<sup>+</sup> upon electrochemical reduction. Because of the stronger acceptor content of this polymer, two reductions attributed to n-type doping are seen. The TBA<sup>+</sup> system has an  $E_{1/2}$  at –1.1 V for the first reduction. The second reduction matches that of TBA<sup>+</sup> doping of poly(1) closely with an  $E_{1/2}$  located at –1.7 V. The smaller TEA<sup>+</sup> also has an  $E_{1/2}$  value of –1.1 V for the first reduction. The second reduction, however, occurs at a slightly more positive value of –1.6 V. Of the electrophilic cations used in this study, only Na<sup>+</sup> displayed a current response in the potential range examined. The  $E_{1/2}$  values associated with the two reductions also behaved as those of the bulkier cations with values of –1.2 V and –1.6 V.

As shown in Scheme 1, the donor–acceptor nature of these structures lead to stabilized charge-separated resonance forms of the undoped polymers hinting at potential stabilized reduction sites. Poly(1) has only one resonance stabilized state indicating that the single nitrogen on the pyridine can only stabilize one negative charge. Of the three donor–acceptor states associated with poly(2), two are localized on the pyrazine ring. The ability of this ring systems to accommodate more electron density than the pyridine ring implies that the first reduction seen in this system is expected to be stabilized here. Since the pyridine ring only stabilizes one electron, the second reduction displayed is expected to appear here. This is verified by the CV data as the second reduction of poly(2) very closely matches that of poly(1) both in onset and  $E_{1/2}$  values.

**X-ray Crystallography.** In order to examine the degree of conjugation and ability to form a planar polymer, an X-ray



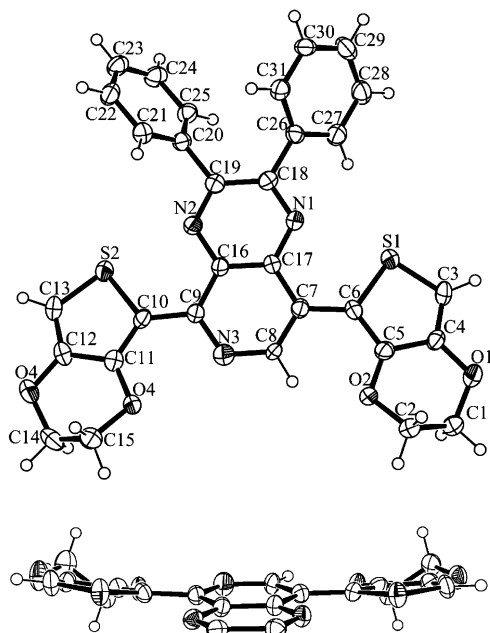


**Figure 3.** Single-crystal X-ray structure of monomer **2**. Top view shows the profile of the monomer. The bottom edge view has the phenyl groups removed for clarity.

crystal structure was obtained of compound **2**. Repeated attempts to grow a single crystal of monomer **1** was unsuccessful because of the compound powdering out rather than forming a crystal. Figure 3 shows that the torsional angle between the EDOT and pyrido[3,4-*b*]pyrazine is very low ( $\sim 3$  and  $7^\circ$ ) as desired for a high level of conjugation. This is demonstrated in the bottom structure where the phenyl rings are removed for clarity. In comparison, BEDOT-benzene has a torsional angle of  $27.5^\circ$  between the EDOT and benzene rings indicating a lower degree of conjugation.<sup>21</sup> Examination of the C6–C7 and C9–C10 bond lengths shows them to be 1.45 and 1.46 Å, respectively. These bond lengths are identical to the bond lengths of BEDOT-benzene with their values being midway between single and double bonds. These values indicate the importance of the resonance structures shown in Scheme 1 along with the added benefit of a highly planar system.

**Polymer Differential-Pulse Voltammetry.** Figure 4 illustrates differential-pulse voltammetry (DPV) behavior of the two polymer systems. DPV offers better sensitivities than CV and leads to sharper peak onsets due to current responses only occurring near the  $E^0$  region.<sup>22</sup> The peak shapes seen in DPV also allude to the redox behavior of the systems. True reversible systems exhibit sharper, more well-defined peaks, while quasi-reversible and irreversible systems give broader peaks. To date, very little work has been done to examine the fundamental behavior of conjugated polymers<sup>23,24</sup> using DPV; rather, efforts have been focused on sensor<sup>25</sup> and release applications.<sup>26</sup>

For poly(**1**), shown in Figure 4A, the oxidation processes have sharper onsets than those associated with cyclic voltammetry yet no peak shape is seen indicating a quasi-reversible process due to capacitive charging of the system. TEAP has an onset of +0.5 V and has the highest current density. NaP has the earliest onset at +0.4 V. LiP displays the smallest current density and the most positive onset at +0.6 V. Of these three electrolytes, only the soft electrolyte shows an appreciable current response upon reduction. Both NaP and LiP have current densities that are indiscernible from background current. TBAP has a current onset of +0.5 V and a current density only slightly smaller than that of TEAP. As with the CV experiment, all

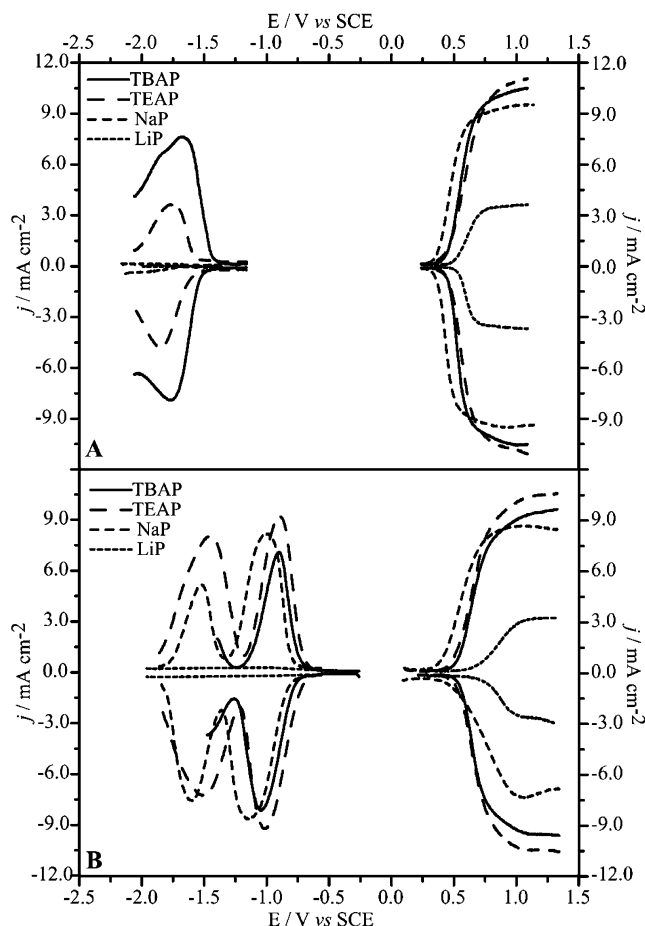


**Figure 4.** Differential-pulse voltammetry of poly(**1**) (A) and poly(**2**) (B) in 0.1 M monomer-free electrolyte solution. The solid line is TBAP, the large dashed line is TEAP, the medium dashed line is NaP, and the small dashed line is LiP. Each polymer was grown cyclically on Pt, rinsed with the appropriate electrolyte solution, and scanned 20 times over the entire potential range to “break-in” the film.

electrolyte systems exhibit color changes from the neutral red to the oxidized navy blue.

Of the electrolyte systems examined, only TBAP and TEAP exhibit current response upon reduction. TBAP displays an onset of  $-1.5$  V with a  $\Delta E$  (difference in peak separation) of 90 mV indicating that the reduction is not truly “reversible.” TEAP also exhibits a  $\Delta E$  of 90 mV with an onset of  $-1.5$  V. As color changes occur only for these two systems, we attribute this to true n-type doping.

As shown in Figure 4B, poly(**2**) behaves similarly to poly(**1**) upon oxidation. TBAP and TEAP have the largest current densities with onsets at +0.6 V. NaP has an onset at 0.4 V and the second largest current density. LiP has the most positive onset at +0.8 V and displays the smallest current density. Relative current densities and onsets for poly(**2**) match those of poly(**1**) quite well indicating that the bis-EDOT donor is not significantly affected by increasing the acceptor strength.

Upon reduction, two processes are seen as shown in Figure 4B. TEAP has onsets at  $-0.7$  V for the first reduction and  $-1.2$  V for the second reduction. The  $\Delta E$  values are 0.1 V for both the first and second reductions. The onsets for NaP are at  $-0.8$  V and  $-1.3$  V with  $\Delta E$  values of 0.2 and 0.1 V. Color changes are seen for both TEAP and TBAP upon conversion from the neutral to the two n-doped states. NaP only exhibits a color change from the neutral to first n-doped state but no second color change to the second reduced state. With LiP, however,

**TABLE 1: Summary of Electrochemical and Conductance Values upon Electrochemical Reduction**

polymer, electrolyte	CV $E_{1/2}$	CV $\Delta E$	DPV onset	DPV $\Delta E$	$\sigma$ onset	$\sigma$ peak
1, TBA <sup>+</sup>	-1.6 V	0.26 V			-1.5 V	0.18 mS
1, TEA <sup>+</sup>	-1.7 V	0.20 V	-1.6 V	0.10 V	-1.6 V	0.31 mS
1, Na <sup>+</sup>					-1.6 V	0.03 mS
1, Li <sup>+</sup>						
2, TBA <sup>+</sup>	-1.1 V, -1.7 V	0.15 V, 0.05 V			-0.8 V, -1.3 V	0.03 mS, 0.06 mS
2, TEA <sup>+</sup>	-1.1 V, -1.6 V	0.15 V, 0.07 V	-0.7 V, -1.1 V	0.12 V, 0.05 V	-0.8 V, -1.3 V	0.07 mS, 0.10 mS
2, Na <sup>+</sup>	-1.2 V, -1.6 V	0.16 V, 0.07 V	-0.8 V, -1.3 V	0.05 V, 0.07 V	-0.8 V	0.25 mS
2, Li <sup>+</sup>					-1.2 V	0.01 mS

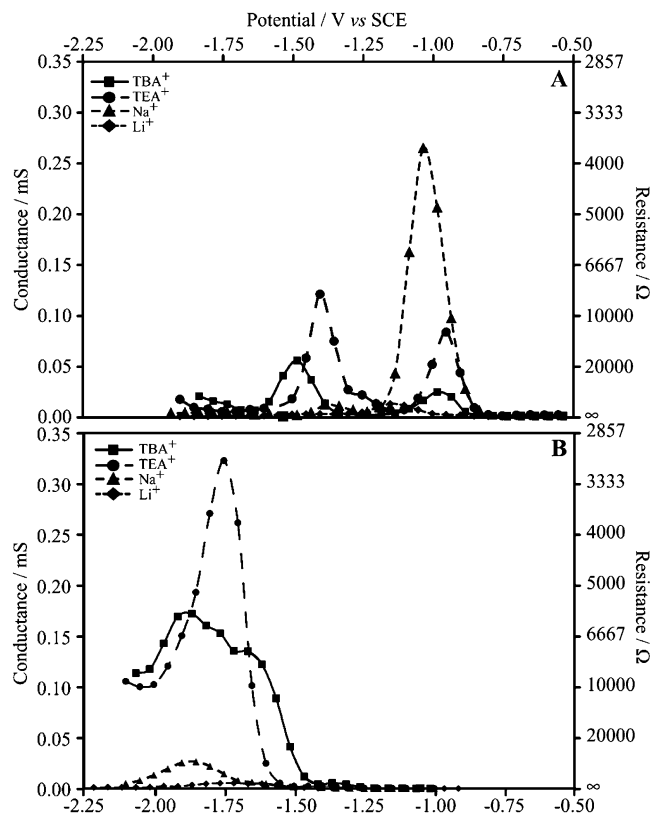


**Figure 5.** In situ conductance of poly(1) (A) and poly(2) (B) in 0.1 M monomer-free electrolyte solution. The solid line is TBAP, the large dashed line is TEAP, the medium dashed line is NaP, and the small dashed line is LiP. Each polymer was grown potentiostatically at 0.1 V negative of  $E_{p,m}$  on a Pt IME, rinsed with the appropriate electrolyte solution, and scanned 20 times over the entire potential range to “break-in” the film before further analysis. (Data shown for TBAP are reprinted with permission from ref 11b. Copyright 2002 Wiley-VCH.)

no color change or redox behavior is seen even when the experiment is conducted out to -1.9 V.

**Polymer Conductivity.** In situ conductance performed on poly(1) further reinforces the CV and DPV results (Figure 5). Of the electrolyte systems examined, only TBAP and TEAP had an appreciable increase in conductance upon reduction with values of 0.18 mS and 0.31 mS, respectively. The onset of the conductance increase occurred at -1.6 V and peaked at -1.8 V before decreasing for TEAP. TBAP had an onset of -1.5 V with a conductance maximum at -1.9 V. Reduction with NaP did lead to a noticeable conductance increase with an onset at -1.6 V, but the peak shifted more negative to almost -1.9 V and only had a conductance of 0.03 mS. LiP had a response undetectable from the background. The only color changes for poly(1) were with the nonelectrophilic TEA and TBA cations.

The results from examination of poly(2) were more startling. NaP had the largest conductance of the electrolyte systems with an onset at -0.8 V and a peak conductance of 0.25 mS at -1.1 V. However, upon further reduction only a small peak is seen

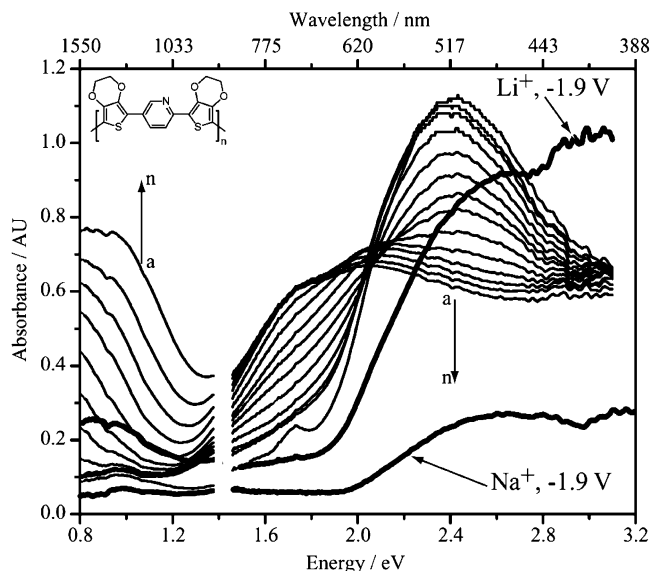


























**Figure 6.** Spectroelectrochemistry of a poly(1) film on an ITO-coated glass slide in monomer-free 0.1 M lithium perchlorate/acetonitrile electrolyte solution. Applied potentials are (a) -1.0, (b) +0.2, (c) +0.3, (d) +0.4, (e) +0.5, (f) +0.6, (g) +0.7, (h) +0.8, (i) +0.9, (j) +1.0, (k) +1.1, (l) +1.2, (m) +1.3, and (n) +1.4 V vs SCE. Bold lines indicate reduction spectra of the polymer film at -1.9 V.

at -1.3 V. TEAP and TBAP had the same onset at -0.8 V as NaP did, but TEAP had a smaller relative conductance of 0.07 mS with a larger peak at -0.9 V. Associated with the second color change is another peak centered at -1.4 V with an onset of -1.3 V and maximum conductance of 0.1 mS. TBAP had a small conductance of 0.03 mS for the first peak and 0.056 mS for the second peak. LiP displayed a rather small conductance of 0.01 mS at -1.2 V. TBAP and TEAP exhibited the expected color changes upon reduction. NaP unexpectedly exhibited color change associated with the first redox peak but none with the second indicating that n-type doping occurs at the first peak, but only redox-type conductivity is seen upon further reduction. This observation further illustrates that n-type doping cannot be discerned by cyclic voltammetry or differential-pulse voltammetry as reduction may occur but not a true n-type doping process. Table 1 summarizes the electrochemical and conductance values.

**Polymer Spectroelectrochemistry.** In order to characterize the reduction of these donor-acceptor-donor polymers, spectroelectrochemical experiments were performed in an argon-filled drybox with a fiber optic coupled CCD and an InGaAs diode array detector. Polymer films were prepared by potentiostatic deposition onto ITO-coated glass slides until charge densities of 25 mC cm<sup>-2</sup> were reached. The spectra are broken into near-IR (NIR) and visible regions as a result of the use of two different detectors.

The spectroelectrochemistry of poly(1) using lithium perchlorate is shown in Figure 6. The  $\pi$ - $\pi^*$  transition is located at 510 nm. Upon incremental oxidation, the absorption transition

**TABLE 2: Color Swatches of Poly(1) and Poly(2) in the Indicated Electrolyte Solutions**

Polymer (electrolyte)	$E_{1/2}$ (ox)	$E_{1/2}$ (red)	oxidized color	neutral color	reduced color	p-doping/ n-doping
<b>1, TBAP</b>	+0.9	-1.8				Yes/Yes
<b>1, TEAP</b>	+1.0	-1.8				Yes/Yes
<b>1, NaP</b>	+0.9	-				Yes/No
<b>1, LiP</b>	+1.0	-				Yes/No
<b>2, TBAP</b>	-	-1.0, -1.7				Yes/Yes
<b>2, TEAP</b>	-	-1.0, -1.5				Yes/No
<b>2, NaP</b>	-	-1.1, -1.6				Yes/No
<b>2, LiP</b>	-	-,-				Yes/No

decreases in intensity as polaron absorption bands increase between 1.5 and 2.0 eV. Full oxidation leads to a bipolaron absorption maximum at 1.0 eV as expected for a polymer that attains high doping levels.

Attempts at reduction spectroelectrochemistry of poly(1) (upper black trace) using the  $\text{Li}^+$  electrolyte solution is much different than p-type doping spectroelectrochemistry, also shown in Figure 6. The absorption associated with the  $\pi-\pi^*$  transition decreases and is bleached, but no intermediate charge carrier formation is observed. This decrease is most likely due to polymer decomposition as highly negative potentials are applied. In the NIR region, the absorption increases slightly, but is not due to bipolaron charge carrier formation indicating no doping process.

Reduction spectroelectrochemistry with sodium perchlorate as the electrolyte is also shown in Figure 6. Its p-doping behavior is identical to that of NaP as expected since perchlorate is the dominant dopant. However, upon application of reductive potentials (lower black trace) no absorption change is seen in the NIR region, and the decrease in visible absorption is attributed to degradation of the polymer because of reductive degradation.

Spectroelectrochemistry of poly(2) using lithium perchlorate is shown in Figure 7. Upon incremental oxidation (Figure 7A), growth of charge carrier bands can be seen at 850 and 1240 nm. The  $\pi-\pi^*$  transition decreases in intensity. However, if reduction potentials are applied, dramatic changes occur relative to p-type doping. All absorptions below 2.25 eV are bleached as potentials are stepped from  $-0.6$  to  $-1.9$  V. The high-energy absorption located at 2.75 eV increases in intensity and becomes slightly red shifted to 2.6 eV. The green neutral color becomes bright orange upon complete reduction. No NIR absorption changes are seen indicating that doping does not occur even though a color change is seen to the orange reduced state.

Spectroelectrochemistry performed with sodium perchlorate is identical in the p-type doping region as the lithium perchlorate. Once again, reductive spectroelectrochemistry is much different than p-type doping. All absorptions below 2.2 eV become completely bleached, and no long wavelength charge carrier

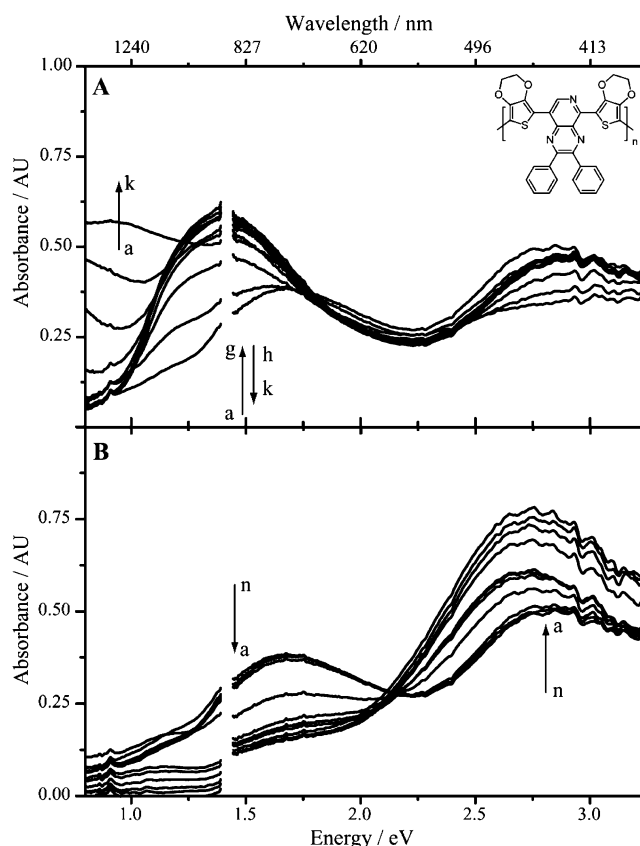


**Figure 7.** Spectroelectrochemistry of a poly(2) film on an ITO-coated glass slide in monomer-free 0.1 M lithium perchlorate/acetonitrile electrolyte solution. p-Type doping (A) applied potentials are (a)  $-0.6$ , (b)  $-0.4$ , (c)  $-0.2$ , (d) 0.0, (e)  $+0.2$ , (f)  $+0.4$ , (g)  $+0.6$ , (h)  $+0.8$ , (i)  $+1.0$ , (j)  $+1.2$ , and (k)  $+1.4$  V vs SCE. n-Type doping (B) applied potentials are (a)  $-0.6$ , (b)  $-0.7$ , (c)  $-0.8$ , (d)  $-0.9$ , (e)  $-1.0$ , (f)  $-1.1$ , (g)  $-1.2$ , (h)  $-1.3$ , (i)  $-1.4$ , (j)  $-1.5$ , (k)  $-1.6$ , (l)  $-1.7$ , (m)  $-1.8$ , and (n)  $-1.9$  V vs SCE.

formation is shown. The absorption peak seen at 2.7 eV increases in intensity and is red shifted to 2.6 eV. No doping

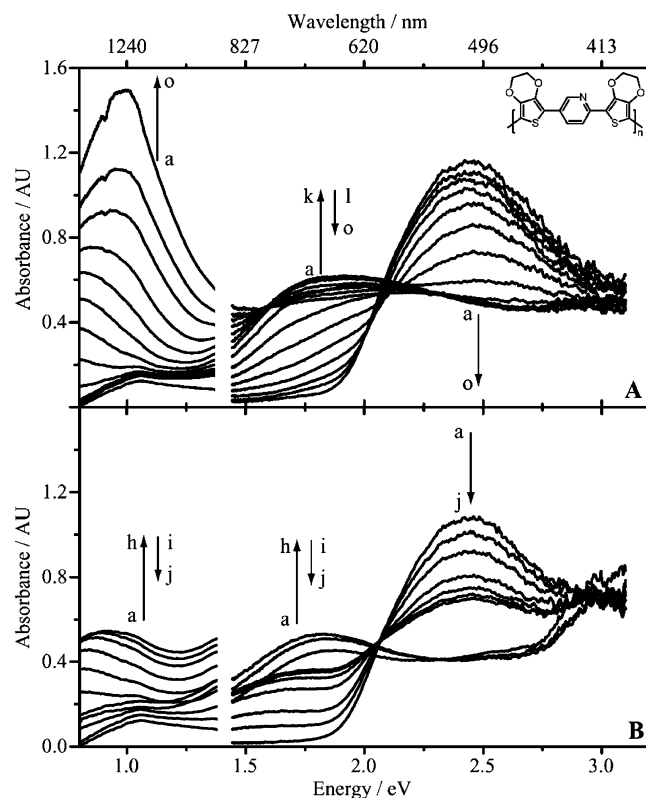


**Figure 8.** Spectroelectrochemistry of a poly(1) film on an ITO-coated glass slide in monomer-free 0.1 M tetra-*n*-ethylammonium perchlorate/ acetonitrile electrolyte solution. p-Type doping (A) applied potentials are (a)  $-0.9$ , (b)  $+0.1$ , (c)  $+0.2$ , (d)  $+0.30$ , (e)  $+0.4$ , (f)  $+0.5$ , (g)  $+0.6$ , (h)  $+0.7$ , (i)  $+0.8$ , (j)  $+0.9$ , (k)  $+1.0$ , (l)  $+1.1$ , (m)  $+1.2$ , (n)  $+1.3$ , and (o)  $+1.4$  V vs SCE. n-Type doping (B) applied potentials are (a)  $-1.0$ , (b)  $-1.1$ , (c)  $-1.2$ , (d)  $-1.3$ , (e)  $-1.5$ , (f)  $-1.5$ , (g)  $-1.6$ , (h)  $-1.7$ , (i)  $-1.8$ , and (j)  $-1.9$  V vs SCE.

process occurs as the film changes from a lime green to a bright orange color.

The p-type doping of poly(1) in TEAP is shown in Figure 8 and has a neutral  $\lambda_{\text{max}}$  near 510 nm (2.4 eV). Preparation of the films in an argon-filled drybox rather than on the benchtop under ambient conditions leads to a 35 nm red shift in  $\lambda_{\text{max}}$  relative to films prepared outside of the drybox due most likely to a lower defect density along the polymeric backbone. Oxidation by stepping potentials in 0.1 V increments from  $-0.9$  to  $0.0$  V leads to no change in optical properties. At  $+0.1$  V, the  $\pi-\pi^*$  transition decreases as an intermediate charge carrier peak forms near 1.75 eV. More complete oxidation occurs at  $+1.4$  V with a decrease in the polaron absorption and substantial growth of a bipolaron absorption band at energies greater than 1.4 eV. This is the biggest enhancement at long wavelength absorption indicating more complete doping.

Examination of n-type doping in TEA<sup>+</sup> electrolyte, shown in Figure 8B, indicates that a similar spectral signature to p-doping occurs, though the nature of the carriers are vastly different. The neutral  $\pi-\pi^*$  transition has a  $\lambda_{\text{max}}$  of 510 nm. As the potential is stepped negative from  $-1.10$  V to  $-1.90$  V, the visible transition decreases steadily until  $-1.70$  V is reached at which point the  $\pi-\pi^*$  transition decreases rapidly and achieves complete depletion with formation of only an intermediate charge carrier band centered at 1.75 eV. One possible explanation for this is the noticeably sharper reduction in the cyclic and differential-pulse voltammetry compared in Figures 3 and 4. Application of more negative potentials leads to a decrease in the low-energy absorptions accounted by the

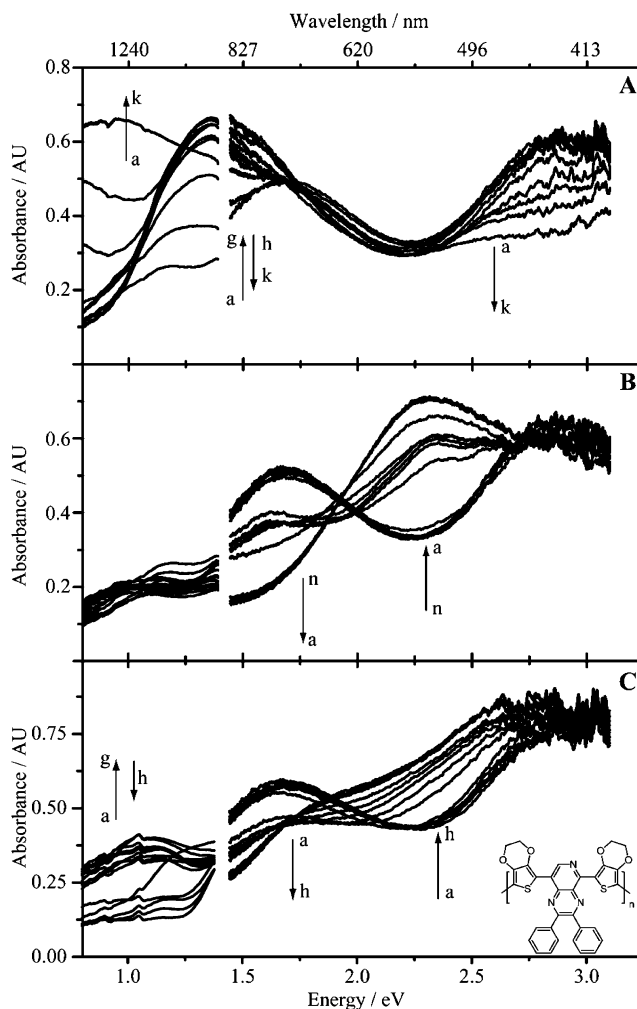


**Figure 9.** Spectroelectrochemistry of a film of poly(2) on an ITO-coated glass slide in monomer-free 0.1 M tetra-*n*-ethylammonium perchlorate/acetonitrile electrolyte solution. p-Type doping (A) applied potentials are (a)  $-0.6$ , (b)  $-0.4$ , (c)  $-0.2$ , (d)  $0.0$ , (e)  $+0.2$ , (f)  $+0.4$ , (g)  $+0.6$ , (h)  $+0.8$ , (i)  $+1.0$ , (j)  $+1.2$ , and (k)  $+1.4$  V vs SCE. n-Type doping (B) applied potentials are (a)  $-0.6$ , (b)  $-0.7$ , (c)  $-0.8$ , (d)  $-0.9$ , (e)  $-1.0$ , (f)  $-1.1$ , (g)  $-1.2$ , (h)  $-1.3$ , (i)  $-1.4$ , (j)  $-1.5$ , (k)  $-1.6$ , (l)  $-1.7$ , (m)  $-1.8$ , and (n)  $-1.9$  V vs SCE. n-Type doping spectroelectrochemistry in TBAP (C) of a poly(2) film is shown with the following potentials: (a)  $-0.5$ , (b)  $-0.7$ , (c)  $-0.9$ , (d)  $-1.1$ , (e)  $-1.3$ , (f)  $-1.5$ , (g)  $-1.7$ , and (h)  $-1.9$  V vs SCE.

degradation of the polymer film. The overall absorbance is slightly lower in intensity and red shifted relative to the oxidized state (0.4 AU vs 1.5 AU) leading to the more transmissive sky blue color. The NIR absorbance is maximum at  $-1.8$  V. Further applied potentials lead to a decrease in absorption as the film degrades as a result of over-reduction. Importantly, the increase in absorbance at long wavelength during reduction indicates formation of charge carriers and true n-type doping.

When the TEAP electrolyte system is used, poly(2) gives similar results to Li<sup>+</sup> (Figure 7) upon p-type doping. The high-energy peak at 435 nm disappears upon oxidation demonstrated in Figure 9. A peak centered above 850 nm grows in as the polymer is oxidized stepwise. As oxidative occurs, an intermediate charge carrier band begins to grow near 900 nm. As further positive potentials are applied, another charge carrier band grows in until broad absorption occurs across the entire NIR region. Upon n-type doping, shown in Figure 9B, the results are more striking. Upon reduction, the  $\pi-\pi^*$  transition at 750–800 nm decreases and a new peak grows in at 545 nm. This gives green to orange color change, similar to that seen in Figure 7B. In



contrast, no change occurs in the NIR upon reduction when potentials up to  $-1.9$  V are applied indicating little doping occurring.

Spectroelectrochemical examination of electrolyte effects of TBAP are similar to TEAP. The neutral absorption gives peaks in the visible region located at 750 nm and near 400 nm. Stepwise oxidation causes decreases in height of both peaks. Upon complete oxidation, a NIR dominant peak occurs that tails into the visible region resulting in the gray-green color of the oxidized film. Examination of the NIR region using TBAP as the electrolyte shows little absorption of the neutral polymer. Upon application of a positive potential, a peak grows rapidly near 900 nm, but upon higher doping levels absorption becomes broad across the entire NIR region.

Upon n-type doping of poly(2) in TBAP, the 750 nm peak decreases in height as doping occurs to give tailing from the blue visible region into the NIR as seen in Figure 9C. The high-energy peak near 400 nm grows in height to give a burgundy red film color upon reduction at  $-1.1$  V and a dark gray upon complete reduction of the film at  $-1.9$  V. Reduction, on the other hand, shows little change in the NIR region. This indicates that the oxidation and reduction processes are different, hence the different colors associated with each redox state. The colors of poly(1) and poly(2) in various electrolyte solutions are summarized in Table 2.

## Summary

Here, we have demonstrated the capability to control both redox and n-type doping processes in a series of bis-EDOT-pyridine polymers by cation effects. Soft, bulky cations, TBA<sup>+</sup> and TEA<sup>+</sup>, cause poly(1) and poly(2) to exhibit true n-type doping based on analysis using cyclic voltammetry, differential-pulse voltammetry, and conductivity experiments. Color changes are observed upon conversion of the polymers from their neutral to n-doped states indicating the formation of charge carriers. Li<sup>+</sup> and Na<sup>+</sup> induce minimal current and conductivity responses for these polymeric systems. No color changes upon reduction are observed with poly(1). Sodium and lithium perchlorate lead to color changes with poly(2) but no charge carrier formation indicating lack of doping. Evidence presented in this paper illustrates that reductive processes are not indicative of true doping in simple electrochemical experiments.

**Acknowledgment.** This project was supported by funding from the Army Research Office/Multi-University Research Initiative (DAAD19-99-1-0316) and the Air Force Office of Scientific Research (AFOSR F49620-03-1-0091). K.A.A. wishes to acknowledge the National Science Foundation and the University of Florida for funding of the purchase of the X-ray equipment.

**Supporting Information Available:** Structure data, atomic coordinates and equivalent isotropic displacement parameters, bond lengths and bond angles, anisotropic displacement parameters, and hydrogen coordinates and isotropic displacement parameters. This material is available free of charge via the Internet at <http://pubs.acs.org>.

## References and Notes

- (1) (a) Würthner, F. *Angew. Chem., Int. Ed.* **2001**, *40*, 1037–1039. (b) Dimitrakopoulos, C. D.; Malenfant, P. R. L. *Adv. Mater.* **2002**, *14*, 99–117.
- (2) (a) Swager, T. M. *Acc. Chem. Res.* **1998**, *31*, 201–207. (b) McQuade, D. T.; Pullen, A. E.; Swager, T. M. *Chem. Rev.* **2000**, *100*, 2537–2574. (c) Albert, K. J.; Lewis, N. S.; Schauer, C. L.; Sotzing, G. A.; Stitzel, S. E.; Vaid, T. P.; Walt, D. R. *Chem. Rev.* **2000**, *100*, 2595–2626.
- (3) (a) McGehee, M. D.; Heeger, A. J. *Adv. Mater.* **2000**, *12*, 1655–1668. (b) Kraft, A.; Grimsdale, A. C.; Holmes, A. B. *Angew. Chem., Int. Ed.* **1998**, *37*, 402–428. (c) Köhler, A.; Wilson, J. S.; Friend, R. H. *Adv. Mater.* **2002**, *14*, 701–707. (d) Hide, H.; Díaz-García, M. A.; Schwartz, B. J.; Heeger, A. J. *Acc. Chem. Res.* **1997**, *30*, 430–436. (e) Dai, L.; Winkler, B.; Dong, L.; Tong, L.; Mau, A. W. H. *Adv. Mater.* **2001**, *13*, 915–925.
- (4) Holdcroft, S. *Adv. Mater.* **2001**, *13*, 1753–1765.
- (5) Novák, P.; Müller, K.; Santhanam, K. S. V.; Haas, O. *Chem. Rev.* **1997**, *97*, 207–281.
- (6) Brabec, C. J.; Sariciftci, N. S.; Hummelen, J. C. *Adv. Funct. Mater.* **2001**, *11*, 15–26.
- (7) (a) Schwendeman, I.; Hwang, J.; Welsh, D. M.; Tanner, D. B.; Reynolds, J. R. *Adv. Mater.* **2001**, *13*, 634–637. (b) Rauh, R. D.; Wang, F.; Reynolds, J. R.; Meeker, D. L. *Electrochim. Acta* **2001**, *46*, 2023–2029. (c) Mortimer, R. J. *Electrochim. Acta* **1999**, *44*, 2971–2981. (d) de Paoli, M.-A.; Casalbore-Miceli, G.; Girotto, E. M.; Gazotti, W. A. *Electrochim. Acta* **1999**, *44*, 2983–2991. (e) Byker, H. J. *Electrochim. Acta* **2001**, *46*, 2015–2022.
- (8) de Leeuw, D. M.; Simenon, M. M. J.; Brown, A. R.; Einerhand, R. E. F. *Synth. Met.* **1997**, *87*, 53–59.
- (9) (a) van Mullekom, H. A. M.; Vekemans, J. A. J. M.; Havinga, E. E.; Meijer, E. W. *Mater. Sci. Eng., R* **2001**, *32*, 1–40. (b) Roncali, J. *Chem. Rev.* **1997**, *97*, 173–205. (c) Roncali, J. J. *Mater. Chem.* **1999**, *9*, 1875–1893.
- (10) For example: (a) Babel, A.; Jenekhe, S. A. *J. Phys. Chem. B* **2002**, *106*, 6129–6132. (b) Alam, M. M.; Jenekhe, S. A. *J. Phys. Chem. B* **2001**, *105*, 2479–2482. (c) Alam, M. M.; Jenekhe, S. A. *Chem. Mater.* **2002**, *14*, 4775–4780.
- (11) (a) Irvin, D. J.; DuBois, C. J., Jr.; Reynolds, J. R. *Chem. Commun.* **1999**, 2121–2122. (b) DuBois, C. J.; Reynolds, J. R. *Adv. Mater.* **2002**, *14*, 1844–1846.
- (12) Aubert, P.-H.; Groenendaal, L.; Louwet, F.; Lutsen, L.; Vanderzande, D.; Zotti, G. *Synth. Met.* **2002**, *126*, 193–198.
- (13) (a) Williams, M. E.; Masui, H.; Long, J. W.; Malik, J.; Murray, R. W. *J. Am. Chem. Soc.* **1997**, *119*, 1997–2005. (b) Long, J. W.; Kim, I. K.; Murray, R. W. *J. Am. Chem. Soc.* **1997**, *119*, 11510–11515. (c) Williams, M. E.; Crooker, J. C.; Pyati, R.; Lyons, L. J.; Murray, R. W. *J. Am. Chem. Soc.* **1997**, *119*, 10249–10250.
- (14) Zotti, G.; Schiavon, G.; Zecchin, S. *Synth. Met.* **1996**, *72*, 275–281.
- (15) Reynolds, J. R.; Schlenoff, J. B.; Chien, J. C. W. *J. Electrochem. Soc.* **1985**, *132*, 1131–1135.
- (16) (a) Schiavon, G.; Sitron, S.; Zotti, G. *Synth. Met.* **1989**, *32*, 209–217. (b) Kittleson, G. P.; White, H. S.; Wrighton, M. S. *J. Am. Chem. Soc.* **1984**, *106*, 7389–7396. (c) Paul, E. W.; Riccio, A. J.; Wrighton, M. S. *J. Phys. Chem.* **1985**, *89*, 1441–1447. (d) Thackeray, J. W.; White, H. S.; Wrighton, M. S. *J. Phys. Chem.* **1985**, *89*, 5133–5140.
- (17) (a) Gritzner, G.; Küta, J. *Pure Appl. Chem.* **1984**, *56*, 462–466. (b) Noviadri, F.; Brown, K. N.; Fleming, D. S.; Gulyas, P. T.; Lay, P. A. Masters, A. I.; Phillips, L. J. *J. Phys. Chem. B* **1999**, *103*, 6713–6722.
- (18) Sheldrick, G. M. *SHELXTL6*; Bruker-AXS: Madison, WI, 2000.
- (19) Groenendaal, L.; Jonas, F.; Freitag, D.; Pielartzik, H.; Reynolds, J. R. *Adv. Mater.* **2000**, *12*, 481–494.
- (20) For example: (a) Yamamoto, T.; Lee, B.-L. *Macromolecules* **2002**, *35*, 2993–2999. (b) Yamamoto, T.; Kanbara, T.; Mori, C.; Wakayama, H.; Fukuda, T.; Inoue, T.; Sasaki, S. *J. Phys. Chem.* **1996**, *100*, 12631–12637. (c) Yamamoto, T.; Maruyama, T.; Zhou, Z.; Ito, T.; Fukuda, T.; Yoneda, Y.; Begum, F.; Ikeda, T.; Sasaki, S.; Takezoe, H.; Fukuda, A.; Kubota, K. *J. Am. Chem. Soc.* **1994**, *116*, 4832–4845. (d) Yamamoto, T.; Sugiyama, K.; Kushida, T.; Inoue, T.; Kanbara, T. *J. Am. Chem. Soc.* **1996**, *118*, 3930–3937. (e) Yamamoto, T.; Zhou, Z.; Kanbara, T.; Shimura, M.; Kizu, K.; Maruyama, T.; Nakamura, Y.; Fukuda, T.; Lee, B.-L.; Ooba, N.; Tomaru, S.; Kurihara, T.; Kaino, T.; Kubota, K.; Sasaki, S. *J. Am. Chem. Soc.* **1996**, *118*, 10389–10399. (f) Kanbara, T.; Yamamoto, T. *Macromolecules* **1993**, *26*, 1975–1979. (g) Lee, B.-L.; Yamamoto, T. *Macromolecules* **1999**, *32*, 1375–1382.
- (21) Sotzing, G. A.; Reynolds, J. R.; Steel, P. J. *Chem. Mater.* **1996**, *8*, 882–889.
- (22) Richardson, D. E.; Taube, H. *Inorg. Chem.* **1981**, *20*, 1278–1285.
- (23) Jin, S.; Cong, S.; Zue, G.; Xiong, H.; Mansdorf, B.; Cheng, S. Z. D. *Adv. Mater.* **2002**, *14*, 1492–1496.
- (24) Nishiumi, T.; Higuchi, M.; Yamamoto, K. *Electrochemistry* **2002**, *70*, 668–670.
- (25) (a) Reynes, O.; Gulon, T.; Moutet, J.-C.; Royal, G.; Saint-Aman, E. *J. Organomet. Chem.* **2002**, *656*, 116–119. (b) Ekinci, E.; Erdogdu, G.; Karagozler, A. E. *J. Appl. Polym. Sci.* **2000**, *79*, 327–332. Ciszewski, A.; Milczarek, G. *Anal. Chem.* **1999**, *71*, 1055–1061. (c) Fabre, B.; Burlet, S.; Cespuoglio, R.; Bidan, G. *J. Electroanal. Chem.* **1997**, *426*, 75–83.
- (26) (a) Diab, N.; Schuhmann, W. *Electrochim. Acta* **2001**, *13*, 860–867. (b) Komura, T.; Kijima, K.; Yamaguchi, T.; Takahashi, K. J. *Electroanal. Chem.* **2000**, *486*, 166–174.